GEOPHYSICAL RESEARCH LETTERS, VOL. 10, NO. 12, PAGES 1137-1140, DECEMBER 1983

THE OCTOBER 1980 EARTHQUAKE SEQUENCE NEAR THE NEW HEBRIDES

John Vidale and Hiroo Kanamori

Seismological Laboratory, California Institute of Technology, Pasadena, California 91125

Abstract. Four large earthquakes occurred in 1980 in a seismic gap near the Loyalty Islands in the New Hebrides. At 3:25 UT on October 24 an event with M_s = 6.7 initiated the sequence. Three events, M_s = 6.7, 7.2, and 6.5, followed on the next day. We investigated this sequence by using the seismicity, first-motion, and waveform data and long-period surface waves. The first-motion data constrain one of each pair of nodal planes. With this constraint, inversion of Rayleigh- and Love-wave spectra at 256 seconds determines the other nodal plane. The mechanisms of all four events are almost pure thrust on a plane dipping about 20 degrees east and striking parallel to the local strike of the New Hebrides trench. The first-day aftershocks indicate an initial rupture zone of about 2,000 km^2, which is consistent with the estimated seismic moment of 3 x 10^{27} dyne-cm. During the next two days, the aftershock activity expanded to an area of 10,000 to 20,000 km^2 in the directions both along and perpendicular to the trench. Within 5 hours after the third and largest event, the initial rupture zone had become mostly quiescent. Modeling of waveforms suggests a body-wave moment of between 0.5 and 1.0 x 10^{27} dyne-cm and a source process time of 11 seconds. This pattern suggests that the initial rupture zone represents a zone of increased strength (i.e. an asperity), and the stress change due to failure of this asperity subsequently migrated outward. During the two-year period before the main event, seismicity in the initial rupture zone was very low except near the point where the first mainshock initiated. A very tight clustering of activity occurred there. This pattern indicates gradual stress concentration near the asperity which finally failed during the mainshock sequence.

Introduction

In October, 1980, an earthquake sequence consisting of 4 large events (M_s = 6.5, 6.7, 6.7, and 7.2; hereafter these events are referred to as the mainshocks) and about 160 aftershocks, which were reported by NEIS (National Earthquake Information Service), occurred in the New Hebrides subduction zone. Figure 1 [McCann, 1980] shows the plate tectonic setting of the region. The black square in the figure contains all the events in the sequence. McCann [1980] assigned the boxed area a seismic potential of 2, which means that the region had experienced an earthquake of M_s greater than 7.0 in the last 100 years but not the last 30 years and has relatively high seismic potential.

In the southern section of the New Hebrides subduction zone earthquakes with M_s of 7.0 to 7.5 appear to recur with at least 30-40 year intervals. Nine events of M_s = 6.5 to 7.5 occurred in the black square between 1943 and 1947 [relocations from McCann, personal communication, 1981; the magnitudes are from Gutenberg and Richter, 1949], but none that large occurred from 1947 to 1980. Because of the uncertainties in the magnitudes of old events, the overall magnitude of the activity from 1943 to 1947 is somewhat uncertain [McCann, personal communication, 1982]. However, recently reevaluated magnitudes of these old events in the southern New Hebrides trench near the Loyalty Islands are smaller than the magnitudes given by Gutenberg and Richter [1949] by only 0.2 units on the average [Abe, 1981]. Thus the activity in 1980 appears similar in magnitude to that in the 1940's. The NOAA catalog lists no earthquakes of magnitude greater than 6 in this region between 1963 and 1979. However, since the sequence in 1980, three shocks of surface-wave magnitude 6.6 or 6.7 have been reported (2/17/81, 9/17/81, and 11/24/81) by NEIS. Also, an event of M_s = 7.3 occurred on 7/6/81 100 km southeast of the region considered in this paper.

Another notable feature associated with this sequence is that the aftershock zone expanded during the first week to an area 10 to 20 times larger than that for the first few hours. Some of the aftershocks occurred near the trench axis. A similar feature has been noted for other events in the New Hebrides [e.g. Isacks et al., 1981]. Also, the aftershock zone during the first few hours became quiescent within six hours after the third mainshock.

Although the relationship between seismicity and the state of stress in the fault zone is not fully understood, recent studies indicate that the spatio-temporal variation of seismicity may reflect the mode of stress buildup, release, and readjustment in the focal zone (see [Lay et al., 1982] for summary). In view of the importance of this sequence as a gap-filling event, we made a detailed analysis of seismicity patterns preceding and following this sequence and of the mechanisms of the mainshocks.

Seismicity

The temporal variation of the seismicity as well as the focal mechanisms, seismic moments, and magnitudes of the four largest earthquakes are shown in Table 1 and Figure 2. The locations of the events are taken from the EDR listings (Earthquake Data Reports, published by NEIS), and the nearest seismic stations used are shown by the x's in Figure 1. The station coverage is good. Coudert et al. [1981] show that the ISC (International Seismological Center) locations and locations from a local seismic network agree to within 10 km for the central portion of the New Hebrides arc. We expect the NEIS location errors to be less than 30 km. Engdahl et al. [1977] showed that location errors of shallow events in subduction zones, if present, will tend to shift apparent earthquake locations toward the island-arc side of the trench, so the existence of events on the oceanside of the trench is probably real.

Focal mechanisms of the four largest events are determined

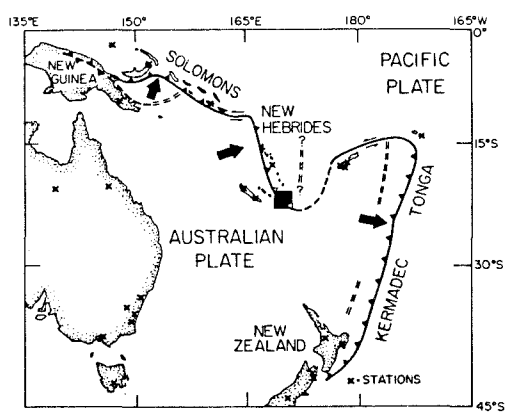

Fig. 1. The tectonic setting of the southwest Pacific ocean. The New Hebrides subduction zone is part of the boundary between the Pacific plate and the Australian plate. The events described in this paper occurred in the black square, near the Loyalty Islands, centered on 170 E and 22 S. The crosses locate the stations used by NEIS for epicenter determination.

Paper number 3L1226.
0094-8276/83/003L-1226$03.00

TABLE 1. Parameters of the Four Largest Events in the Sequence

Date	Time (GMT)	Moment (in 10^{27} dyne-cm)	Latitude (degrees)	Longitude (degrees)	First Nodal Plane (Strike)	(Dip)	Second Nodal Plane (Strike)	(Dip)
10/24/80	3:25	.20	-21.989	170.165	321	20	141	70
10/25/80	7:00	.46	-21.982	170.025	316	30	136	60
10/25/80	11:00	2.00	-21.890	169.853	322	25	142	65
10/25/80	16:20	.10	-22.313	170.380	297	20	117	70

from long-period WWSSN (Worldwide Standardized Seismograph Network), IDA (International Deployment of Accelerometers), and SRO (Seismic Research Observatories) and ASRO (Abbreviated Seismic Research Observatories) records. First motions from WWSSN film chips constrain the more steeply dipping nodal plane. With this one nodal plane constrained, the amplitude and phase spectra of Rayleigh and Love waves at a period of 256 seconds obtained from IDA, SRO, and ASRO data are inverted by the method described in Kanamori and Given [1981].

The mechanisms of the four largest events are indistinguishable from pure thrust (Figure 2). The first mainshock with M_s = 6.7 and seismic moment of 2 x 10^{26} dyne-cm occurred at 3:25 UT on October 24, 1980, and was followed by the second mainshock with M_s = 6.7 and seismic moment of 4 x 10^{26} dyne-cm at 7:00 UT on the next day. Figure 2d shows the locations of these first two earthquakes and their aftershocks, which preceded the third and largest event. The third event occurred four hours after the second, with M_s = 7.2 and moment of 2 x 10^{27} dyne-cm. Figure 2e shows the activity from the third main event until 5 hours later. The fourth mainshock (with M_s = 6.5, shown in Figure 2a) has a smaller moment of 1 x 10^{26} dyne-cm and may be considered to be an aftershock of the third mainshock. The distribution of events from 5 hours after the largest event until December 31, 1980, is shown in Figure 2f. All the events that occurred in the first week had depths listed as less than 33 km.

The source time function and the body-wave moment of the third event are estimated by comparison of the observed and synthetic seismograms. The observed waveforms are digitized from film chips of long-period WWSSN records for COL (College, Alaska), KIP (Kipapa, Hawaii), LON (Longmire, Washington), and MSO (Missoula, Montana). The synthetic seismograms are computed from a simple dislocation model as described in Kanamori and Stewart [1976]. The mechanism listed in Table 1 is used for the third event. A homogeneous half space is assumed, and direct P, pP, and sP phases are included in the synthetics. We assume a point source at a depth of 15 km and use a symmetric trapezoidal time function with the rise time t_0 and effective width t_1 (i.e., total width $t_0 + t_1$; see Figure 3). Figure 3 shows the observed records as well as the synthetics for three source time functions with (t_0 = 3 sec, t_1 = 8 sec), (4, 11), and (5, 14). The source time function with (t_0 = 4 sec, t_1 = 11 sec) fits the observed records best.

The amplitudes of the records for COL, KIP, LON, and MSO yield body-wave moments of 0.56, 0.96, 0.72, and 0.44 x 10^{27} dyne-cm, respectively, with an average of 0.6 x 10^{27} dyne-cm. A second source of body-wave radiation with about one-third the amplitude of the first pulse may be seen about 50 seconds after the first arrival on the observed records. The body-wave moment is about 30% of the 256 second period surface-wave moment of 2 x 10^{27} dyne-cm. Although there is some trade-off between the depth, the shape of the source time function, and the moment, we will use the values obtained here (the effective width of the source time function = 11 sec, the seismic moment = 0.6 x 10^{27} dyne-cm) as gross parameters of the body-wave source.

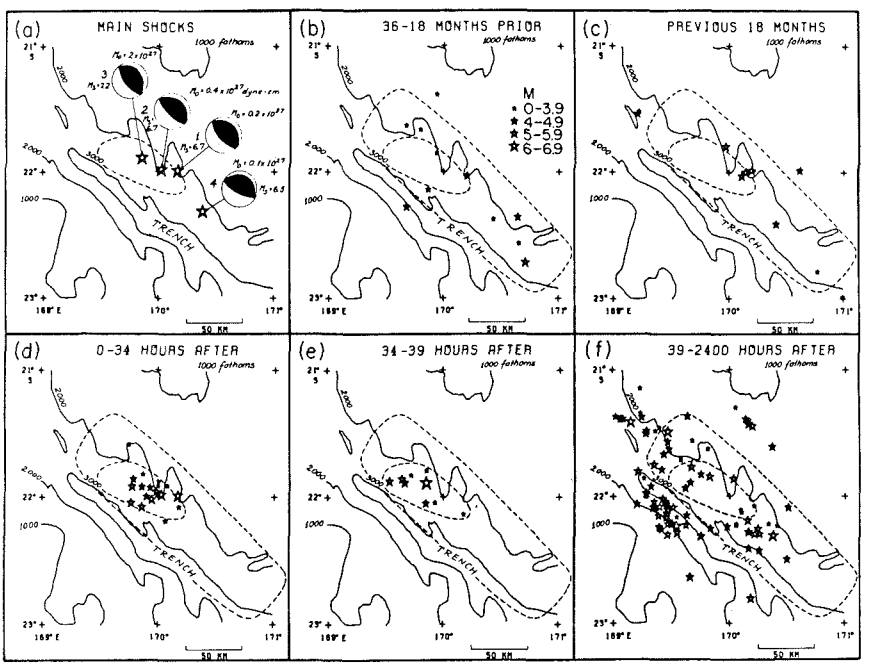

Fig. 2. Seismicity plots of the area covered by the black square in Figure 1. Stars indicate earthquakes; larger symbols indicate larger events. The solid lines contour the bathymetry (Mammerickx et al., 1974) in fathoms. Figure 2a shows the hypocenters, mechanisms, surface-wave magnitudes, and seismic moments for the four largest events in the sequence. Figures 2b and 2f show activity in 5 different time windows. The outer dotted line contains the later aftershock zone and was derived from Figure 2f. The inner dotted line contains the immediate aftershock zone and was drawn from Figure 2e.

Discussion

The aftershock area was about 2000 km^2 immediately after the third event (Figure 2e) and expanded to fill an area of about 15,000 km^2 in the following week. We exclude both the area oceanward of the trench and the area so far to the east that the shallow aftershocks could not have been on the interplate boundary.

The spreading pattern could indicate several different rupture mechanisms. The first possible mechanism is that the immediate aftershock area (the smaller area defined by dotted lines in Figure 2), which is much smaller than the later aftershock area (the larger area defined in Figure 2), may be the entire extent of the coseismic rupture, and the later aftershock area is in response to a slow diffusion of the stress change from the mainshocks outward through a zone of viscous material. The total moment M_o of the three largest events in the sequence is 2.7 x 10^{27} dyne-cm. If the coseismic slip took place over the immediate aftershock area shown in Figure 2e, the amount of slip D would be

$$D=M_o/\mu A=3.2m \quad (1)$$

where μ is the rigidity (here 5 x 10^{11} dyne/cm^2 is used) and A is the size of the immediate aftershock area, which is estimated to be 2000 km^2 from Figure 2e. If the thrust plane between the Australian and Pacific plates had been completely locked during the interseismic period and the interval is about 30 years, the convergence rate of 10 cm/yr [Dubois et al., 1977] would cause accumulated slip of 3 m, which is approximately equal to the coseismic slip estimated above.

As mentioned earlier, the average body-wave moment, 0.6 x 10^{27} dyne-cm, is significantly smaller than that obtained from the surface waves, suggesting that the body-wave source is much smaller than the surface-wave source. Although the size of the body-wave source cannot be determined accurately, the effective width of 11 sec indicates a source dimension of about 22 km if unilateral rupture with a velocity of 2 km/sec is assumed. This dimension is considerably smaller than that of the immediate aftershock area. If the rupture is bilateral or circular, the dimension of the body-wave source could be as large as 44 km, but it is still considerably smaller than that of the immediate aftershock area.

The result that the moment and the source area estimated from body-waves are smaller than those from surface waves is not unusual, especially for large earthquakes in some subduction zones.

An alternative possibility is that the entire later aftershock area could have ruptured in the mainshocks, but the average displacement was only about 30 cm instead of 3 meters. If this is the case, the absence of earthquakes in the prior 35 years in the black square in Figure 1 requires either that 9/10 of the slip has been aseismic or that much of the fault plane slips in several earthquakes during an earthquake cycle.

Although either one of these cases or a combination of them is possible, we consider the first case most satisfactory in view of the good agreement between the amount of coseismic slip estimated from the seismic moment and that predicted by plate motion. We use this model in the rest of this paper.

The other striking feature is the expansion of the zone of quiescence near the center, which grew to a radius of 50 km by the end of the first week. This feature can be seen in Figures 2d, 2e, and 2f, where a zone of quiescence develops in the area of the inner dotted line, which represents most of the immediate aftershock zone.

The development of quiescence in the immediate aftershock area may reflect the difference in mechanical properties between the immediate aftershock area and the surrounding area. In terms of the mechanism proposed above, the immediate aftershock area is more brittle (undergoes less aseismic slip) than the surrounding area, so that stress readjustment after the mainshock may have been completed quickly, resulting in a shorter duration of aftershock activity.

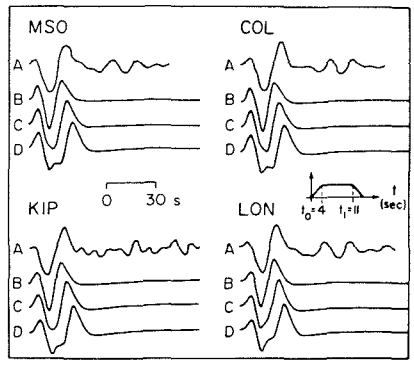

Fig. 3. Body-wave synthetics for 4 WWSSN stations. Trace A in each group is the observed seismogram. Traces B have a trapezoidal time function of (t_0 = 3 sec, t_1 = 8 sec) as illustrated schematically in the figure and as discussed in the text. Traces C and D have time functions of (4,11) and (5,14)

Conclusion

In our preferred model, the immediate aftershock area that broke in the first three events (M_s = 6.7, 6.7, 7.2) represents a stronger section of the fault zone, where most of the preseismic stress accumulation took place. In this sense, we call this area a fault asperity [see e.g. Lay et al., 1982]. Within the asperity, there is an even stronger region. When the strongest region breaks, body-wave and long-period surface-wave energy is radiated. The rupture subsequently propagates into the rest of the asperity, which then radiates the rest of the long-period surface-wave energy but little body-wave energy, except possibly for the small arrival 50 seconds into the record (visible in Figure 3). The effect subsequently propagates outward, causing expansion of the aftershock activity.

With this asperity model, we interpret the seismicity patterns in the area before the mainshocks. Figure 2c shows the activity during the 18-month period before the mainshocks. Clustering of the events near the point of initial rupture (epicenter of the first event) seems to indicate stress concentration on one edge of the asperity, perhaps in the strongest region. During the 18-month period prior to this period (Figure 2b), no obvious seismicity pattern is found that may indicate the existence of the asperity.

Although this interpretation is not unique, the accurate determinations of seismic moments together with spatio-temporal mapping of seismicity provide an important clue to the distribution and the nature of asperities that control the mode of stress accumulation leading to a large earthquake. Detailed information on the location and the character of an asperity such as the one indicated by Figure 2e and identification of clustering activity such as the one shown in Figure 2c are important for evaluating the seismic potential of a gap.

For long-term earthquake prediction, areas with the potential for large earthquakes can be identified on the basis of seismic gaps [McCann, 1980]. In the intermediate term, the gaps could be monitored for large areas of quiescence and clustering of events to indicate areas that might rupture and the point where rupture might initiate, respectively.

Acknowledgments. This work was partly supported by USGS contract No. 14-08-0001-21223. We thank Jeff Given for providing us with computer programs. William McCann generously supplied a preprint of his paper, some of his data, and permission to use a figure from his paper. Larry Ruff, Thorne Lay, and Jim Pechmann provided valuable advice. The figures were drafted skillfully by Laszlo Lenches. J.E.V. was supported by a Gutenberg Fellowship and an NSF Fellowship. The IDA data were provided by the IDA Project team at the University of California, San Diego, and the SRO and ASRO data were provided by the U.S. Geological Survey. Contribution 3856 of the Division of

Geological and Planetary Sciences, California Institute of Technology, Pasadena, California 91125.

References

Abe, K., Magnitudes of large shallow earthquakes from 1904 to 1980, *Phys. Earth Planet. Inter., 27*, 72-92, 1981.

Coudert, E., B. L. Isacks, M. Barazangi, R. Louat, R. Cardwell, A. Chen, J. Dubois, G. Latham, and B. Pontoise, Spatial distribution and mechanisms of earthquakes in the southern New Hebrides arc from a temporary land and ocean bottom seismic network and from worldwide observations, *J. Geophys. Res., 86*, 5905-25, 1981.

Dubois, J., J. Dupont, A. Lapouille, and J. Recy, Lithospheric bulge and thickening of the lithosphere with age: examples in the Southwest Pacific, in *International Symposium on Geodynamics in the Southwest Pacific*, pp. 371-380, Technip, Paris, 1977.

Engdahl, E. R., N. Sleep, and M. Lin, Plate effects in northern Pacific subduction zones, *Tectonophysics, 37*, 95-116, 1977.

Gutenberg, B., and C. F. Richter, *Seismicity of the Earth*, Princeton Univ. Press, Princeton, 273 pp., 1949.

Isacks, B., R. Cardwell, J. Chatelain, M. Barazangi, J. Marthelot, D. Chinn, and R. Louat, Seismicity and tectonics of the central New Hebrides island arc, in *Ewing Conf. Symposium on Earthquake Prediction*, edited by D. W. Simpson and P. G. Richards, pp. 97-101, Am. Geophys. Union, Washington, D.C., 1981.

Kanamori, H., and J. W. Given, Use of long-period surface waves for rapid determination of earthquake-source parameters, *Phys. Earth Planet. Inter., 27*, 8-31, 1981.

Kanamori, H., and G. S. Stewart, Mode of strain release along the Gibbs fracture zone, Mid-Atlantic ridge, *Phys. Earth Planet. Inter., 11*, 311-32, 1976.

Lay, T., H. Kanamori, and L. Ruff, The asperity model and the nature of large subduction zone earthquakes, *Earthquake Prediction Research, 1*, 35-103, 1982.

Mammerickx, J., T. E. Chase, S. M. Smith, and I. L. Taylor, *Bathymetry of the South Pacific*, Chart No. 12 of 21, Scripps Inst. of Oceanography, La Jolla, Calif., 1974.

McCann, W. R., Large- and moderate-size earthquakes; their relationship to the tectonics of subduction, Ph.D. thesis, 194 pp., Columbia Univ., New York, 1980.

(Received June 28, 1983;
accepted July 19, 1983.)